Review

Continuation of periodic orbits in symmetric Hamiltonian and conservative systems

J. Galan-Vioque[1,a], F.J.M. Almaraz[2], and E.F. Macías[1]

[1] Departamento de Matemática Aplicada II e Instituto de Matemáticas de la Universidad de Sevilla, Camino de los Descubrimientos s/n, Sevilla 41092, Spain
[2] Departamento de Ciencias Físicas, Matemáticas y de la Computación, Universidad Cardenal Herrera, San Bartolomé 55, 46115 Alfara del Patriarca – Valencia, Spain

Abstract. We present and review results on the continuation and bifurcation of periodic solutions in conservative, reversible and Hamiltonian systems in the presence of symmetries. In particular we show how two-point boundary value problem continuation software can be used to compute families of periodic solutions of symmetric Hamiltonian systems. The technique is introduced with a very simple model example (the mathematical pendulum), justified with a theoretical continuation result and then applied to two non trivial examples: the non integrable spring pendulum and the continuation of the figure eight solution of the three body problem.

1 Introduction

It is well known that the bifurcation of periodic orbits constitute the backbone of a Hamiltonian system. If we succeed in analyzing the branching and stability behavior of these solutions as the parameters or the energy are varied, we can hope to understand and predict the general evolution of systems with symmetries and conserved quantities.

Nature, at its most basic level, has decided to be Hamiltonian; non-Hamiltonian systems come up in Physics only as phenomenological models for the more complicated underlying processes. However, Hamiltonian systems are non generic dynamical systems with remarkable properties, in particular with respect to periodic orbits. The role of periodic solutions in Hamiltonian systems and their importance in modern physics was first recognized by Poincaré [1]; and nowadays they are at the basis of both classical and quantum mechanics [2]. Poincaré conjectured that periodic orbits, i.e. solutions which return to their initial conditions after some finite time, are densely distributed among all possible bounded classical trajectories; and he suggested that the study of periodic orbits would provide the clue to the overall behavior of any mechanical system.

In this paper we review some results on the continuation and bifurcation of periodic orbits in conservative systems and show how two-point boundary value problem

---

[a] e-mail: `jgv@us.es`

continuation software can help us to disclose the fortress Poincaré was talking about in his *Methodes Novelles*, by providing an efficient tool to compute families of periodic orbits in Hamiltonian systems and to discover numerically how these families bifurcate and connect. We will in particular pay attention to symmetric Hamiltonian systems, where the symmetries and the associated first integrals typically increase the dimension of these families.

The work is organized as follows. In Sect. 2 we discuss several aspects of periodic orbits in Hamiltonian systems, in particular how they are organized in families and how one can approach the numerical calculation of these families. In Sect. 3 we give an outline of theoretical continuation results for periodic orbits and relative equilibria; these results include a set-up for the equations which can be used for numerical computations. In Sect. 4 the method is illustrated with a paradigmatic toy example; the mathematical pendulum. In Sect. 5 we present the first non trivial application of our continuation results for a non integrable spring pendulum. In Sect. 6 we present continuation results for the three-body problem, starting from the figure eight for the case with equal masses, and using one of the masses as (an external) continuation parameter; we show that the starting solutions can be continuously connected to a periodic solution of the restricted three-body problem. We finish with some general conclusions.

2 Periodic solutions in Hamiltonian systems

It is well known that general (dissipative) and Hamiltonian (or more generally conservative) systems behave quite differently with respect to periodic orbits, their continuation and their bifurcations. In dissipative systems periodic orbits are generically isolated (limit cycles), and therefore an external parameter is required in order to be able to continue such periodic orbits. For Hamiltonian systems there is the celebrated *cylinder theorem* (see [3] or [8] and Fig. 1) which says that periodic orbits appear in one- or more-parameter families, and that under appropriate non-degeneracy conditions these families are persistent under small Hamiltonian perturbations.

In Fig. 1 we plot a schematic representation of the cylinder theorem and the reduction technique. The initial value p generates a periodic orbit (in blue) that belongs to a family that can be parameterized by the conserved quantity F (usually the energy) which is schematically represented by the orange surface which locally resembles a cylinder. We can study the dynamic around the solution by fixing the value of F (magenta plane) or if want to vary the F with a hyperplane transversal to the orbit along the cylinder (green plane π). In both cases we can reduce the dimension of the problem.

The computational problem of finding a periodic orbit can be formulated as a boundary value (or shooting) problem with the period as an additional parameter. In order to avoid phase shifts and to ensure uniqueness one has to introduce an appropriate phase condition which can be either a boundary condition (Poincaré type condition) or an integral version of it (see [5] for more details). In dissipative systems this problem is generically well determined: the periodicity condition together with the phase condition give $n + 1$ equations (n = dimension of the phase space) for the n components of the initial point, the period and the external parameter; generically these equations can be solved by the Implicit Function Theorem, giving a one-dimensional solution curve which can be parametrized by the external parameter.

This scheme no longer works for Hamiltonian systems or, more generally, for systems having a first integral. (Also time-reversible systems are exceptional, but we will not consider those in detail since they require different arguments). In conservative systems periodic orbits typically belong to one parameter families, parametrized by
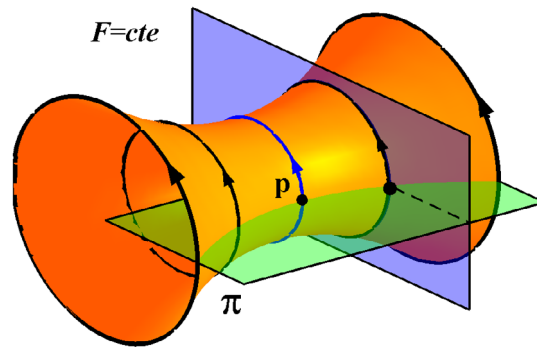
Fig. 1. Schematic representation of the cylinder theorem and the reduction technique. The initial value p generates a periodic orbit (in blue) that belongs to a family that can be parameterized by the conserved quantity F which is schematically represented by the orange surface which locally resembles a cylinder. We can study the dynamic around the solution by fixing the value of F (magenta plane) or if want to vary the F with a hyperplane transversal to the orbit along the cylinder (green plane π).

the value of the first integral (the energy in the Hamiltonian case). This "internal" or "natural" parameter is not explicitly available in the equations, at least not directly, and this makes the standard continuation scheme to fail. Additional complications arise for Hamiltonian systems having several independent constants of motion (symmetries according to Noether theorem [8]): here periodic orbits belong to families having the dimension of the number of independent integrals, and further "phase conditions" are required in order to uniquely identify members of such family. In the next subsection we describe how one can handle this difficulty.

3 Continuation of periodic orbits in conservative systems

A straightforward approach for the continuation is to use the conserved quantity (the energy, in the Hamiltonian case), to eliminate one of the variables; then we choose a suitable Poincaré section for the flow, and look for fixed points of the corresponding Poincaré map. This scheme usually based on shooting methods can be extended to the case of several constants of motion and has been extensively used in the literature, see, for example, [6]. It requires numerical integration of the differential equations, which can give errors in case of very stiff equations for very unstable orbits. The section must be adapted at each step in the continuation process to ensure transversality. This approach also makes it difficult to use integral phase constraints which have often significant computational advantages over the classical Poincaré phase condition. The idea underlying this scheme is that of the *reduction* of the dimension of the problem by making use of the conserved quantities and/or the symmetries; it is a direct translation of the standard theoretical treatment of the problem. A classical example is the N-body problem (see e.g. [7]) that will be discussed later in this paper.

The approach which we propose here **increases** the dimension rather than reducing it, and reformulates the problem in a form where boundary value continuation methods can be applied directly. Our formulation not only allows to prove and extend some basic continuation results for periodic orbits in Hamiltonian systems – such as the "cylinder theorem" of [8] – but can also be implemented directly for the numerical calculation of branches of periodic orbits.

Our starting point will be a generalization of some continuation results of Sepulchre and MacKay for periodic orbits of systems having a first integral; in [9] these

authors introduce the concept of a *normal periodic orbit* and show that such normal periodic orbits belong to one-parameter families of normal periodic orbits. The key idea of their approach is to embed the conservative equation in a one-parameter family of dissipative systems by adding a small gradient perturbation term to the vector field in such a way that a periodic orbit of the perturbed system can only exist when the perturbation is zero. Properly speaking the added term acts more as an **unfolding term** than as a perturbation. Under the normality condition one can invoke the Implicit Function Theorem to obtain a continuation result for periodic orbits of the extended system; because of the just mentioned property of the perturbation this means that in fact one has a continuation result for the unperturbed conservative system.

The idea of adding a dissipative term which allows periodic orbits only when the dissipation is zero is not new; it is for example used in one of the classical proofs of the Lyapunov Center Theorem, where this theorem is shown to correspond to a vertical Hopf bifurcation (see e.g. [10]). Numerically the idea has been used in, for example, the thesis of Zufiría [11], the paper [12] by Aronson et al., and several other papers.

To be more precise, consider a smooth n-dimensional vector field $g : \mathbb{R}^n \to \mathbb{R}^n$, and assume that the corresponding system

$$\dot{u} = g(u) \tag{1}$$

has a nontrivial first integral $F : \mathbb{R}^n \to \mathbb{R}$, i.e. each orbit of (1) is contained in a level set of F, and consequently $\nabla F(u) \cdot g(u) \equiv 0$. Let $u_0(t)$ be a periodic solution of (1), with initial point $p_0 := u_0(0)$, minimal period $T_0 > 0$, and *monodromy matrix* M (this monodromy matrix is given by $M = V(T_0)$, where $V : \mathbb{R} \to \mathcal{L}(\mathbb{R}^n)$ is the transition matrix for the variational equation $\dot{v} = Dg(u_0(t)) \cdot v$; the eigenvalues of M are the *multipliers* of the periodic solution $u_0(t)$). Assuming that $\nabla F(p_0) \neq 0$ one can show that 1 is an eigenvalue of M with geometric multiplicity $m_g \geq 1$ and algebraic multiplicity $m_a \geq 2$ (full proofs are in [13]). In order to continue the periodic solution $u_0(t)$ we replace the Eq. (1) by the extended equation

$$\dot{u} = T\left[g(u) + \alpha \nabla F(u)\right], \tag{2}$$

which depends on two (real) parameters T and α. We will look for 1-periodic solutions $u(t)$ of (2), with $(u(0), T, \alpha)$ near $(p_0, T_0, 0)$. The basic remark is that such solution can only exist for $\alpha = 0$, since

$$0 = F(u(1)) - F(u(0)) = \int_0^1 \nabla F(u(t)) \cdot \dot{u}(t)\, dt = \alpha T \int_0^1 \|\nabla F(u(t))\|^2\, dt;$$

the integral at the right hand side is different from zero ($\nabla F(u(0))$ is close to $\nabla F(p_0) \neq 0$), and hence α must be zero. We conclude that a 1-periodic solution of (2) corresponds (after an appropriate time rescaling) to a T-periodic solution of (1).

Denote the flow of (2) by $\tilde{u}(t; p, T, \alpha)$ ($p \in \mathbb{R}^n$ is the initial value). To find the 1-periodic solutions we are looking for we must impose the periodicity condition $\tilde{u}(1; p, T, \alpha) = p$; to avoid phase shifts we must also impose a phase condition. Therefore we define a mapping $G : \mathbb{R}^n \times \mathbb{R} \times \mathbb{R} \to \mathbb{R}^n \times \mathbb{R}$ by

$$G(p, T, \alpha) := (\tilde{u}(1; p, T, \alpha) - p, \langle g(p_0), p - p_0 \rangle), \tag{3}$$

($\langle \cdot, \cdot \rangle$ is any scalar product on $\mathbb{R}^n$); by hypothesis we have $G(p_0, T_0, 0) = 0$, and we look for zeros (p, T, α) of G near $(p_0, T_0, 0)$. Using the implicit function theorem in combination with the remark above one can then prove the following.

Theorem 1. *Let $u_0(t)$ be a periodic solution of the conservative Eq. (1), with initial point $p_0 = u_0(0)$, minimal period $T_0 > 0$ and monodromy matrix M. Assume that $\nabla F(p_0) \neq 0$ and that 1 is an eigenvalue of M with geometric multiplicity $m_g = 1$. Then the solution set of the equation $G(p, T, \alpha) = 0$ consists locally near $(p_0, T_0, 0)$ of a unique smooth curve along which $\alpha \equiv 0$. More precisely, this solution curve can be written in the form $\{(p^*(T), T, 0) \mid T \text{ near } T_0\}$ for some smooth $p^* : \mathbb{R} \to \mathbb{R}^n$ such that $p^*(T_0) = p_0$.*

This theorem is essentially a restatement of the cylinder theorem for conservative systems (see [8]) in a form which is adapted to numerical implementation; it forms the simplest case of a more general continuation result for conservative systems which can be found in [13].

The condition $m_g = 1$ of Theorem 1 can not be satisfied in case the Eq. (1) has several independent first integrals; then the more general theory of [13] is required. This is in particular the case for continuation in the N-body problem, where next to the Hamiltonian also the components of the total linear momentum and the total angular momentum are first integrals; we refer to Sect. 6 for examples.

It is worth to mention that the theorem can be extended in two directions:

– Further simplifications both in the theory and in the implementation can be achieved if reversibilities are present [14] and [15]. In this case only a portion of the orbit has to be considered and the emanating branches can be selected by imposing the appropriate boundary conditions according to the reversibility (see Sect. 5 for an example).
– For the case of k independent conserved quantities (see Sect. 6 for an application).

For the numerical implementation of Theorem 1 (or similar results) the periodicity condition $\tilde{u}(1; p, T, \alpha) = p$ is usually replaced by a boundary value problem for the full solution $u(t)$ $(0 \leq t \leq 1)$, and the Poincaré type phase condition is replaced by an integral version. Setting $\tilde{u}_0(t) := \tilde{u}(t; p_0, T_0, 0) = u_0(T_0 t)$ this leads then to a boundary value problem of the following form:

– (**CON-1**)Find $(u(t), T, \alpha)$ near $(\tilde{u}_0(t), T_0, 0)$ such that

$$\begin{cases} \dot{u}(t) = T\left[g(u(t)) + \alpha \nabla F(u(t))\right], \\ u(1) = u(0), \\ \int_0^1 \langle \dot{\tilde{u}}_0(t)), u(t) - \tilde{u}_0(t) \rangle \, dt = 0. \end{cases} \tag{4}$$

4 A model example: The mathematical pendulum

In this section we show for illustration some results of the numerical implementation of the foregoing approach to a particular simple example, namely the mathematical pendulum. While discussing this example we put some emphasis on several numerical issues related to such numerical implementation.

The dimensionless mathematical pendulum $\ddot{\theta} + \sin\theta = 0$, that can be written a first order ODE systems as:

$$\begin{aligned} \dot{x}_1 &= x_2, \\ \dot{x}_2 &= -\sin(x_1). \end{aligned} \tag{5}$$

It is a one degree of freedom Hamiltonian system, corresponding to the Hamiltonian $H(x_1, x_2) = \frac{1}{2}x_2^2 + 1 - \cos(x_1)$. The variable x_1 represents the angular displacement from the vertical axis (θ) (so $x_1 \in S^1 = \mathbb{R}/2\pi\mathbb{Z}$), and x_2 the angular velocity $(\dot{\theta})$; the Hamiltonian has been chosen such that the equilibrium at the origin, corresponding to the stable hanging solution, has zero energy.

It is well known that this equation has a family of periodic orbits, originating at the origin and terminating at a homoclinic orbit to the saddle point $(\pi, 0)$, and corresponding to librations of the pendulum; Fig. 2 (upper right) shows some representative orbits. This family can be parametrized by either the energy, or the period (which increases monotonically from 2π to infinity), or the maximal angular displacement; however, neither one of these quantities is explicitly available in the Eq. (5). As we have observed before, such behaviour (which is non-generic for general, dissipative systems) is typical for Hamiltonian (or more generally, conservative) systems. Beyond this homoclinic solutions there exist non periodic solutions (in the $\theta, \dot{\theta}$ variables) that correspond to rotations around the suspension point.

In order to calculate the family of librating periodic solutions we follow the approach outlined in the previous subsection and replace (5) by (a time rescaled version of) the system

$$\begin{aligned} \dot{x}_1 &= x_2 + \alpha \sin(x_1), \\ \dot{x}_2 &= -\sin(x_1) + \alpha x_2. \end{aligned} \tag{6}$$

This system still has two equilibria, the origin which is a stable or an unstable focus depending on the sign of α, and the saddle $(\pi, 0)$. For all non-equilibrium solutions $(x_1(t), x_2(t))$ the function $h(t) := H(x_1(t), x_2(t))$ is strictly decreasing if $\alpha < 0$ or strictly increasing if $\alpha > 0$; this excludes periodic solutions for $\alpha \neq 0$, which agrees with the theoretical results and is also confirmed by a phase plane analysis of (6). So periodic solutions are only possible for $\alpha = 0$ in which case (6) coincides with (5) and we have the family of periodic orbits mentionned before. The bifurcation diagram for periodic orbits of (6) therefore looks as in the top left panel of Fig. 2; this diagram very much ressembles that of a classical Hopf bifurcation, except that in this case the bifurcating branch is completely vertical. It is also clear that α can not be used to parametrize the family of periodic orbits.

Computationally the Eq. (6) has the desired form, with one external parameter. Starting the computation from, for example, $\alpha = -1$ and with initial point $(x_1, x_2) = (0, 0)$, a software package such as AUTO ([16,17]) will locate $(\alpha, x_1, x_2) = (0, 0, 0)$ as a Hopf bifurcation point from the trivial solution and, after switching branches, compute the "vertical branch" of periodic orbits. Along this branch the value of α, computed as part of the solution for each continuation step, appears to be zero (up to numerical precision). The results of such computation are illustrated in Fig. 2; in particular, the center and bottom left panels of this figure illustrate the fact that the "internal parameter" H (the energy) or the period can be used to parametrize the family of periodic orbits.

Some further remarks on the numerical implementation are in order.

– In the pseudo-arclength continuation technique used by AUTO there is no "distinguished parameter"; in our particular example α is just one of the quantities which have to be computed at each continuation step. This allows (for example) the computation along folds and, as illustrated by the current example, the continuation of vertical solution branches.
– Orthogonal collocation with adaptive mesh selection is used to solve the boundary value problem at each continuation step. In Fig. 2 bottom right we show how the time step varies along the orbit: it shrinks at places where the solution varies rapidly whereas it remains large at slowly varying parts of the orbit. This allows to compute the family up to orbits with large period, i.e. very close to the homoclinic orbit that terminates the branch (see Fig. 2 center left).
– The integral phase condition keeps the regions of rapid variation of the solution component x_2 at practically the same location when the period becomes large, as can be seen in Fig. 2 (centre right). This allows bigger continuation steps to
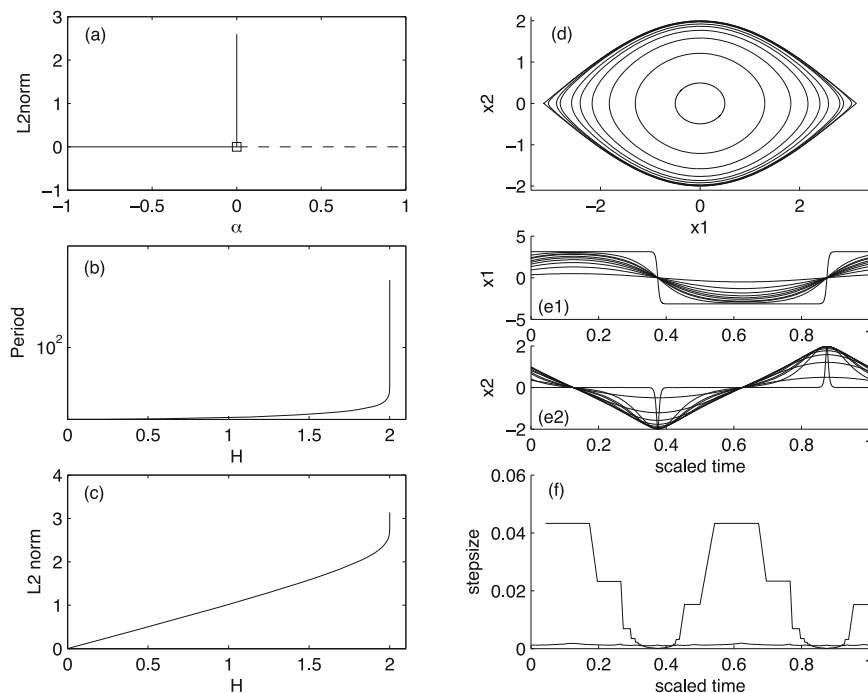
Fig. 2. Continuation results for the mathematical pendulum. The bifurcation diagram obtained by sweeping the parameter α across zero corresponds to a "vertical Hopf bifurcation" (top left). The phase portrait in the top right panel shows 10 different periodic orbits from the one-parameter family. The origin is a center and the unstable equilibria (saddle points) correspond to the inverted pendulum. Center left and bottom left we plot the period and the L_2-norm of the solutions versus the energy; the period is plotted in a logarithmic scale and goes up to above 10^3 using moderate time meshes ($\sim$100 mesh points). The L_2 norm goes from zero to π, which is the value corresponding to the homoclinic solution. In the center right panels we plot the time evolution of the x_1 and x_2 variables. Observe that the use of an integral phase condition results in "freezing" the positions of the "dips" in the solutions. The bottom right panel shows the evolution of the time step along the orbit for a solution "far" from the homoclinic solution (orbit number 5 counting from the origin in the phase portrait), and a second one "very close" to the homoclinic connection. Note how the time step adapts itself to the variations of the solution.

be taken compared to phase conditions that allow the dip to move. For further details on this particular aspect of the computations see [18] and [5].

5 First application: The spring pendulum

As a first non trivial mechanical example we apply the previous method to the spring pendulum of Fig. 3 where we make use of cartesian coordinates q_1 and q_2. A mass (bob) which can move in a plane under the action of gravity is hanging from a weightless elastic spring (shaft) with one of its ends fixed at the origin. The generic motion is a combination of libration or rotation for the pendulum and elastic oscillation for the spring (depending on the energy which depends on the initial condition). A celestial mechanics approach to the elastic pendulum can be found in [19], whereas an extensive numerical treatment of the problem and references can be found in [20].
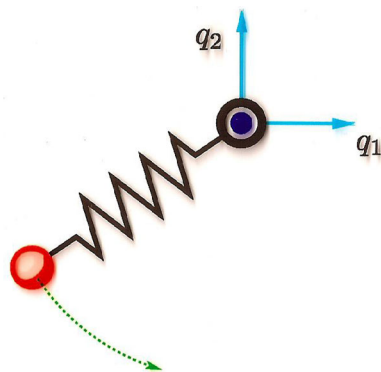
Fig. 3. Spring Pendulum in cartesial coordinates q_1 and q_2. A mass (the red bob) which can move in a plane under the action of gravity is hanging from a weightless elastic spring (the black shaft) with one of its ends fixed at the origin. The generic motion is a combination of libration or rotation for the pendulum and elastic oscillation for the spring.

It is surprising how two integrable systems with very simple behavior considered separately may exhibit extremely complex behavior when they are able to interact and exchange energy among the modes. One of the sub-systems (the spring) is isochronous whereas the other (pendulum) is known to have a increasing period of oscillation (see previous section). In fact we may expect to find resonances between the modes as either the parameters or the energy (internal parameter) are varied. The role of resonances and energy transfer for this problem can be found in [21].

The correct modeling of the spring pendulum requires the inclusion of the *rest length* L_0 of the spring which represents the length at which the spring is neither compressed nor extended. In fact, it can be shown [22] that the most convenient adimensional parameter is precisely $\lambda = \frac{L_0 k}{mg}$.

The dimensionless Hamiltonian (energy) of the system is

$$H = \frac{p_1^2}{2} + \frac{p_2^2}{2} + \frac{1}{2}(\sqrt{q_1^2 + q_2^2} - \lambda)^2 + q_2 + \lambda + \frac{1}{2},$$

where the potential energy is a sum of the elastic term (with the square root) and gravity (q_2) the final constant term has been chosen so that the hanging solution is a zero energy for all values of λ. There is a single explicit continuation parameter λ.

The equations of motion can be derived as usually in Hamiltonian dynamics and involve a denominator that will vanish at the origin. This fact is due to the singularity that reflects the fact that a spring cannot compressed to zero length and has not been always considered in the literature. It is worth to mention that the problem becomes trivial for the case $\lambda = 0$ because it is **linear**. This happens exactly at the $1 : 1$ resonance.

The system exhibits two equilibria for $q_1 = 0, q_2 = -\lambda - 1$ (the hanging position) which is stable and present for all values of λ, and $q_1 = 0, q_2 = -\lambda - 1$ which is always unstable and present only for $\lambda > 1$ that corresponds to the case in which the spring is strong enough to support the weight of the bob it the upright position. The energy is the only conserved quantity of the two degrees of freedom problem and the non integrability of the system has been proven by using the Morales-Ramis theory [23].

An interesting and illuminating numerical exercise is to directly implement the reduction technique to produce the so called Poincaré section for a given value of the energy. We need to define a plane transversal to the trajectories, integrate the system starting from a large number of initial conditions and detect all the intersections of
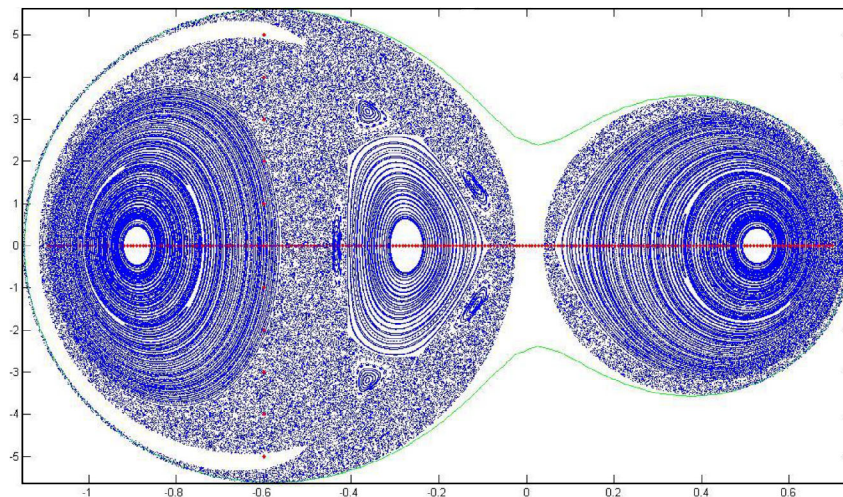
Fig. 4. Poncaré section of the dynamics of a set of initial conditions corresponding to a fixed value of the energy. The horizontal direction is the q_2 axis and the vertical axis is $\dot{q}_2$. The green curve surrounding the whole cloud is the border of the allowed set of initial conditions compatible with the energy level. We have fixed the energy at a high value and three regions of "concentric" curves are visible, that represent tori. The middle one corresponds to the solutions around the stable hanging equilibrium and the two exterior ones to rotating solutions. The unstructured cloud of points around those tori correspond to chaotic trajectories and the origin is avoided in agreement with its singular character.

the trajectories with the chosen plane in a preselected direction **for the same level of energy**. As the original system lives in a four dimensional space and we eliminate one variable ($\dot{q}_1$) from the energy condition and another from the intersection with the plane ($q_1 = 0$), the dynamics is reduced to a set of points in a plane. An example is shown in Fig. 4, where the horizontal direction corresponds to the q_2 axis and the vertical axis is $\dot{q}_2$. A different scaling for the Hamiltonian was used in this computations [20]. The green curve surrounding the whole cloud is the border of the allowed set of initial conditions compatible with the energy level. In this case we have fixed the value of the energy at a high value and three regions of "concentric" curves are visible, that represent tori. The middle one corresponds to the solutions around the stable hanging equilibrium and the two exterior ones to rotating solutions. The unstructured cloud of points around those tori correspond to chaotic trajectories and the origin is avoided in agreement with its singular character. The expected KAM structure with elliptic and hyperbolic solutions is also present.

This diagrams should be computed for many initial conditions and many values of the energy with high accuracy to illustrate the dynamics of the system. Fortunately, it is an *embarrassingly parallelizable* problem that can be efficiently computed using Taylor methods with machine precision accuracy and event location [24–26]. An animation of the evolution of the Poincaré section can be found in [27].

 The theoretical and numerical scheme presented in 3 can be directly applied to the stable hanging pendulum solution. The Lyapunov Center Theorem [8], under non resonant conditions provide two families of stable periodic solution with known period related to the imaginary part of the eigenvalues of the linearization around the equilibrium point.

Along any of this family we can compute the *characteristic multipliers* that control the stability and bifurcation behavior as shown in Fig. 5. The upper left panel is the
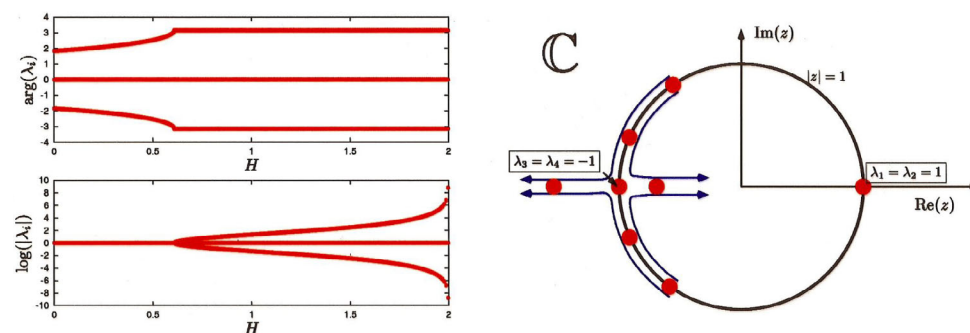
Fig. 5. Characterist or Floquet multiplier as a function of the value of the energy for a splitting Period Doubling bifurcation. The upper left panel is the complex argument of the multipliers as a function of the energy (Hamiltonian value) whereas the lower left panel displays the log of the modulus of the multipliers; a vanishing value implies that the multiplier is **on the unit circle** (elliptic solution). The right panel shows the path of the multiplier in the complex plane with the unit circle as a guide to the eye.
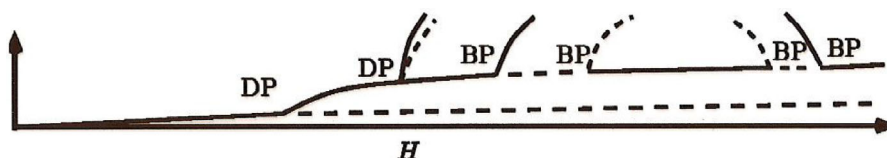

Fig. 6. Schematic bifurcation diagram of the family of periodic solution originated at the vertical solution of the spring pendulum. The horizontal axis is the energy and the vertical is a scalar measure of the solution (the L_2 norm). DP stands for period doubling whereas BP is a branching point. A solid line represents a stable branch (elliptic) whereas a dashed line corresponds to an unstable one (hyperbollic). The main branch corresponds to the harmonic oscillator solution with $q1 = \dot{q1} = 0$ which is stable until a period doubling occurs. The emanating branch exhibits a rich and complex behavior with several bifurcating branches.

complex argument of the multipliers as a function of the energy (Hamiltonian value) whereas the lower left panel displays the log of the modulus of the multipliers; a vanishing value implies that the multiplier is **on the unit circle** (elliptic solution). The right panel shows the path of the multiplier in the complex plane with the unit circle as a guide to the eye. In this case, we present a splitting Period Doubling bifurcation where a pair of Floquet multipliers move on the unit circle, meet at -1, and depart at the unit circle. It could also remain on the unit circle (passing period doubling). It is well known [8] that if μ is a multiplier then $1/\mu$ is also a multiplier. This explain the symmetry of the figure.

The schematic bifurcation diagram is presented in Fig. 6 where splitting and passing period doubling and branching point are observed. A solid line represents an elliptic branch whereas the dashed denotes a hyperbolic (unstable) branch. More details can be found in [22].

The spring pendulum has two reversibilities; the natural one ($R_1 : p_1 \to -p_1$, $p_2 \to -p_2$ and $t \to -t$) and the combination with the $\mathbb{Z}_2$ symmetry ($R_2 : q_1 \to -q_1$, $p_2 \to -p_2$ and $t \to -t$), and both can be used to continue reversible periodic solutions.

In Figs. 7 and 8 we present the continuation results when the reversibility is included in the boundary value formulation (see [15] and [22] for the details). Only a portion of the periodic solution need to be computed since the rest is recovered by applying the corresponding reversibility. The plane where the families are drawn is
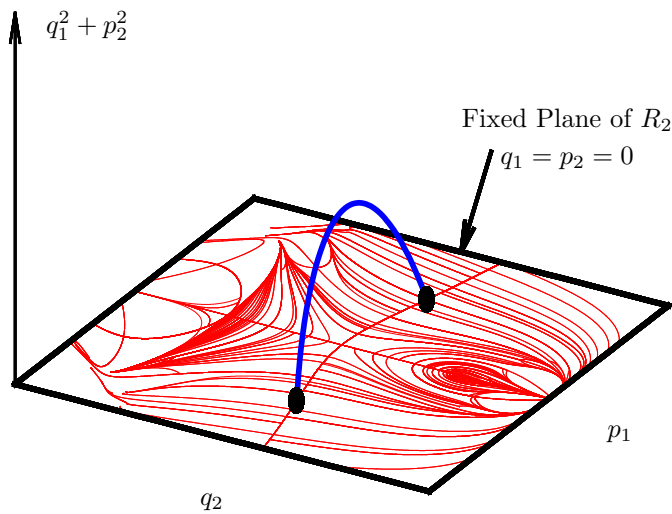
Fig. 7. Representation of the continuation of reversible periodic solutions as a boundary value problem on the fixed plane of the reversibility ($p_1 - q_2$). The vertical axis is a scalar measure of the solution. Along the continuation only a portion of the orbit has to be considered (the blue curve). A reversible solution intersects twice with the fixed plane of the reversibility and the different bifurcating families of reversible solutions represented by this double intersections draw a symmetric plot in the horizontal plane.

the fixed plane of the reversibility and allows an appealing way to follow and classify the families. Note that a reversible periodic solution intersects twice the fixed plane.

In particular Fig. 8 is the R_2 reversible continuation of the periodic solution emanating form the equilibrium. The red curves are the normal modes and the blue curves are associated to bifurcating solutions. The connections between the different branches and the limiting cases correspond to the periodic solutions that were identified in the Poincaré sections for varying values of the energy. The non periodic (quasi periodic or chaotic) are not represented in this bifurcation diagram but can be anticipated by a combined study with characteristic multipliers. Both approaches (Poincaré section and bifurcation diagrams) are complementary and should be undertaken simultaneously.

6 Second application: Continuation of the figure eight solution

Celestial Mechanics has been at the origin of the theory of dynamical systems and many of the techniques from that theory were developed to analyze the fascinating behavior of a group of massive bodies under the influence of their mutual gravitational interaction.

In this section we apply our continuation scheme to a very particular solution of the Three Body Problem (3BP). Part of these results were obtained in collaboration with A. Vanderbauwhede and E.J. Doedel and were published in [28,29].

The spectacular discovery by Chenciner and Montgomery [30] of the existence of a new solution of the 3BP with equal masses in which all three bodies follow the same planar curve with the shape of a "figure eight" has brought great excitement to the dynamical systems community; the origin of the name of the orbit becomes apparent from a real space representation such as in Fig. 10 (top). This solution was first discovered (numerically) by Moore [31] in the context of a study of possible braid
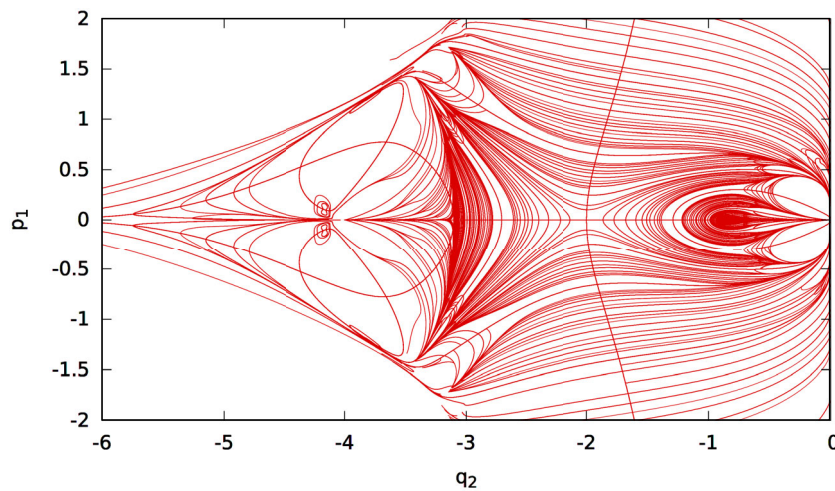
Fig. 8. Continuation of R_2 reversible families of periodic solutions emanating form the origin for $\lambda = 1$. The curves emanating form $(-2,0)$ are the normal modes (vertical harmonic oscillations and the pendular librations) and the rest of the curves are associated to bifurcating solutions. This way of plotting the families provides an organized and appealing way to represent the rich and complex bifurcating behavior of the periodic solutions in the spring pendulum.

types associated to the planar N-body problem. The method of proof by Chenciner and Montgomery is based on variational arguments; after some reductions the action integral is minimized on a restricted set of symmetric arcs to prove the existence of a solution in which the three bodies of equal masses chase each other following a closed trajectory. However, the variational proof is unable to decide about the stability of the solution.

Simó [32] computed this remarkable solution numerically with great accuracy and announced *elliptic stability*; i.e. the nontrivial characteristic multipliers of the periodic orbit are on the unit circle. The precise values of the nontrivial characteristic multipliers (those which are different from one) are given by $\mu_j = exp(2\pi i \nu_j)$ ($j = 1, 2$), with $\nu_1 = 0.00842272$ and $\nu_2 = 0.29809253$. Note that the smallness of ν_1 indicates that the Fig. 8 solution is close to a bifurcation. Simó [33] also discovered many (hundreds) other similar "choreographic solutions" for three equal bodies, and for N equal bodies with $3 < N < 799$ ([32]); the defining property of such *choreography* is that all bodies follow a single closed curve in phase space, with a fixed delay between each of the bodies.

From the historical point of view the solution found by Lagrange in 1772, in which the three bodies form the vertices of an equilateral triangle which rotates with constant angular velocity around its midpoint, can be considered as the first choreography. It has taken more than two hundred years to find the second one.

Our original motivation to study this problem was a conjecture by Joe and Herb Keller on the possibility to connect these two simple choreographies (Lagrange and Figure Eight) in a continuous way only following periodic orbits. In fact, Marchal [34] has found a family of periodic orbits in a *rotating frame* connecting these two highly symmetrical solutions.

A further reason for trying to connect the Lagrange and Figure Eight choreographies has to do with some controversy about the stability properties of the solution corresponding to the absolute minimizer of the action over certain homotopy classes of loops in configuration space. In Hamiltonian systems with two degrees of freedom,

such minimizing orbits are always unstable [35]; however, for higher dimensional systems there are counterexamples.

The stable Fig. 8 orbit was obtained by minimizing the action over all loops with a particular symmetry (see [30]); assuming that the property "minimizing orbits are unstable" also holds for equal mass 3BP there must exist some other unstable periodic orbit which is in the homotopy class of the Fig. 8 but which has a lower action.

Could this orbit be the equilateral Lagrange choreography?

It is unstable, and its action value ($3\pi 3^{2/3} \approx 19.60436$ when the period equals 2π) is lower than that of the figure-8 (≈ 24.37197); but we do not know whether it is in the homotopy class of the figure-8. If it is not (as suggested by Offin [36]) then the minimizer over this homotopy class has to be some other unstable periodic orbit which will then probably not be a choreography. Finding some connection between the figure-8 and the Lagrange orbit could at least give some partial answers to this general question.

We have applied the general continuation scheme of Sect. 3 using the numerically computed figure-8 orbit as starting solution. The equations of motion of three bodies with masses m_1, m_2 and m_3 under mutual gravitational attraction take the form

$$
\begin{aligned}
\ddot{\mathbf{x}}_1 &= -m_2 \frac{\mathbf{x}_1 - \mathbf{x}_2}{|\mathbf{x}_1 - \mathbf{x}_2|^3} - m_3 \frac{\mathbf{x}_1 - \mathbf{x}_3}{|\mathbf{x}_1 - \mathbf{x}_3|^3}, \\
\ddot{\mathbf{x}}_2 &= -m_1 \frac{\mathbf{x}_2 - \mathbf{x}_1}{|\mathbf{x}_1 - \mathbf{x}_2|^3} - m_3 \frac{\mathbf{x}_2 - \mathbf{x}_3}{|\mathbf{x}_2 - \mathbf{x}_3|^3}, \\
\ddot{\mathbf{x}}_3 &= -m_1 \frac{\mathbf{x}_3 - \mathbf{x}_1}{|\mathbf{x}_1 - \mathbf{x}_3|^3} - m_2 \frac{\mathbf{x}_3 - \mathbf{x}_2}{|\mathbf{x}_3 - \mathbf{x}_2|^3};
\end{aligned} \tag{7}
$$

$\mathbf{x}_i = (x_i, y_i, z_i) \in \mathbb{R}^3$ denotes the position of the i-th body ($i = 1, 2, 3$), and the universal gravitational constant has been set equal to 1. This system can be rewritten as a first order system of dimension eighteen. There are seven independent conserved quantities: the total energy, the three components of the total linear momentum $\mathbf{P} = \sum_{i=1}^3 m_i \dot{\mathbf{x}}_i$, and the three components of the total angular momentum $\mathbf{L} = \sum_{i=1}^3 m_i \mathbf{x}_i \wedge \dot{\mathbf{x}}_i$; these are an immediate consequence of the invariance of the equations under time shifts, translations and rotations.

Additionally, the equations are invariant under the transformation $(t, \mathbf{x}) \mapsto (c^{\frac{3}{2}} t, c\mathbf{x})$, with $c > 0$ an arbitrary constant (see [7]). Due to this scaling property there is a trivial continuation of periodic orbits in the period: arbitrary close to any periodic orbits there is another one with slightly different period obtained from the first one by rescaling and obviously with the same stability properties. In order to avoid this trivial continuation we fix the period (say to 2π) and use instead the mass m_1 of the first body as an external continuation parameter; both other masses are kept equal to 1. It is not difficult to check numerically that the figure-8 orbit (corresponding to $m_1 = 1$) is normal (we have $m_g = k = 7$), and hence we can apply Theorem 1, with $\lambda = m_1$. As already discussed before, when setting up the continuation algorithm the phase conditions are replaced by integral versions; for the detailed computational formulation we refer to [28].

The calculations were done using AUTO ([16] and [17]). While following a one-parameter family of periodic orbits we also monitor the stability of these orbits and the appearance of new branches at bifurcation points; at such bifurcation points AUTO allows to switch branches and start a new continuation process. This combination of local stability and bifurcation analysis with global path following forms a valuable approach, complementary to numerical simulations.

Starting at the figure-8 solution for $m_1 = 1$ the first output of our continuation algorithm are the non-trivial characteristic multipliers of this figure-8 solution; we
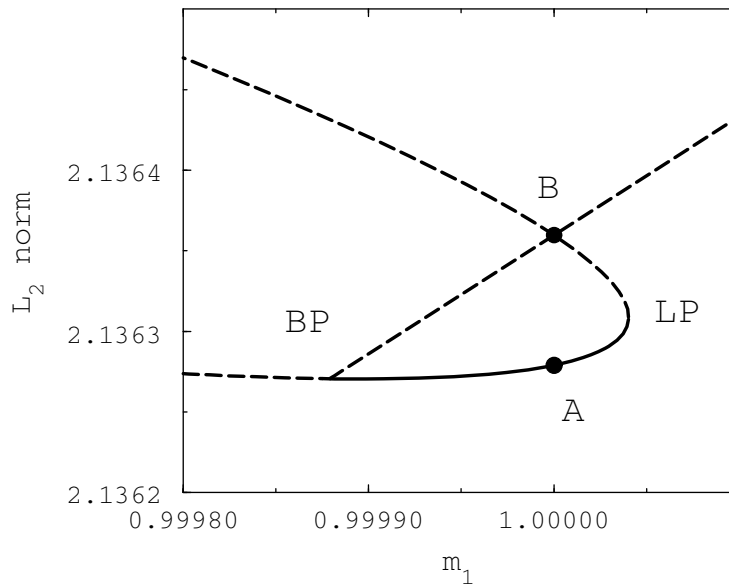
Fig. 9. Local bifurcation diagram near the figure-8 solution under variation of the mass m_1. Solutions on the full part of the curve are stable, those on dashed curves unstable. Stable solutions appear in a narrow window between a pitchfork bifurcation (BP) and a limit point (LP). There are two orbits for the Three Body Problem with equal masses ($m_1 = 1$): label A indicates the stable Chenciner-Montgomery figure-8 solution shown in the upper panel of Fig. 10, label B corresponds to the unstable "satellite" figure-8 shown in the lower panel of Fig. 10.

obtain $\mu_j = \exp(2\pi i\nu_j)$ $(j = 1, 2)$, with $\nu_1 = 0.0084227$ and $\nu_2 = 0.2980925$. The agreement with the results of Simó [32] forms a good test for our method.

The results of the continuation of the figure-8 in a small mass interval around $m_1 = 1$ is shown in Fig. 9 where the L_2-norm of the solution is plotted against m_1. The solution labelled **A** is the starting point of our calculation (the Moore-Chenciner-Montgomery figure-8); this planar orbit is plotted in real space in the upper panel of Fig. 10. Decreasing m_1 from $m_1 = 1$ we obtain a single solution branch which shows a pitchfork bifurcation at (BP), while increasing m_1 gives a solution branch which reaches a limit point (LP) and then continues in the direction of decreasing values of m_1. All solutions along the branch are unstable (hyperbolic), except those on the part of the branch between the bifurcation point (BP) and the limit point (LP), where the solutions are stable (elliptic); this stable part of the branch corresponds to a very narrow mass (m_1) interval of the order 10^{-5}. Continuing the branch beyond the limit point we come back to a situation where all three masses are equal ($m_1 = 1$). The corresponding solution, labeled **B** in Fig. 9, is hyperbolic and by construction in the same homotopy class as the figure-8; however, it has less symmetry and is no longer a choreography: as shown in the lower panel of Fig. 10 the three bodies follow three slightly different figure-8 paths. This "satellite figure-8" solutions was also computed numerically by Simó [33].

At the bifurcation point (BP) there is a pitchfork bifurcation at which the interchange symmetry of the 2nd and 3rd body (which both have the same mass $m_2 = m_3 = 1$) is broken; at the bifurcation two symmetry related branches are born which are represented by a single line in Fig. 9. Along these branches the solutions are hyperbolic and the mass m_1 increases. Also along these branches one finds a special point where $m_1 = 1$ and which therefore corresponds to three equal masses; the
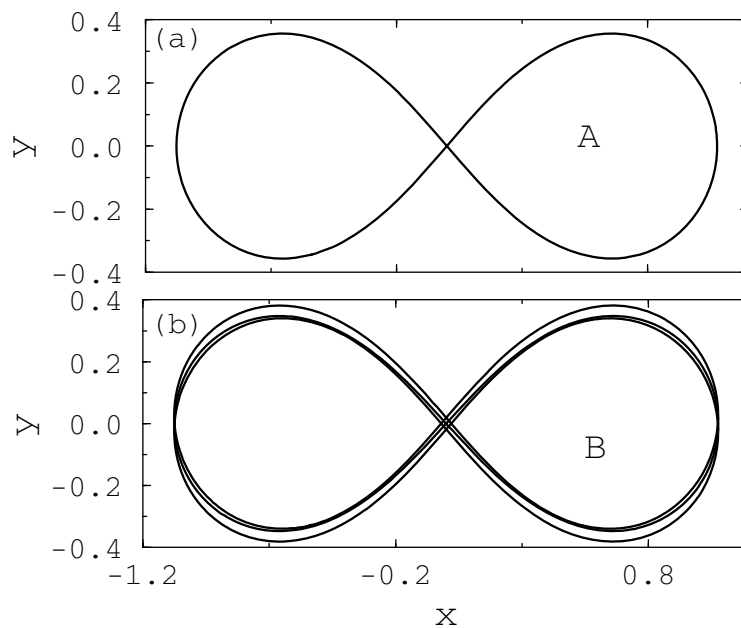
Fig. 10. Real space representation of the figure-8 solution (A) and the other unstable solution (B) for the Three Body Problem with equal masses.

corresponding solutions are the same as the solution **B** described before and shown in the lower panel of Fig. 10, however with a different labelling of the three bodies. The intersection of the three branches at **B** is only apparent and an artifact of the chosen representation.

It is clear from (7) that by choosing appropriate units one can always assume that $m_3 = 1$, leaving m_1 and m_2 as (dimensionless) parameters. Since the figure-8 solution (corresponding to $m_1 = m_2 = 1$) is normal it can be continued in both these parameters, using a multi-parameter version of Theorem 1. When this is done and the stability of the orbits on the continuation is studied (numerically) one obtains a picture as shown in Fig. 11. The shaded triangular region forms the stability region in the (m_1, m_2)-plane, i.e. for mass values (m_1, m_2) in this shaded region the continuation of the figure-8 orbit is elliptic; the point labelled **A** in the center corresponds to the figure-8. Along the border of this stability region (the solid line) the continuation manifold exhibits a fold (limit point); the two points labelled **BP** correspond to branch (bifurcation) points. The diagram is obviously symmetric with respect to the diagonal $m_1 = m_2$; this is a consequence of the invariance of the equations under the symmetry $(\mathbf{x}_1, \mathbf{x}_2, m_1, m_2) \mapsto (\mathbf{x}_2, \mathbf{x}_1, m_2, m_1)$.

In principle one could try to continue the figure-8 solution into a solution of the restricted three body problem by going along the diagonal and increasing the value of $m_1 = m_2$; in practice one finds that as the two equal masses become larger the bodies collide. The results is shown in Fig. 12 where the global bifurcation diagram of the family of periodic solutions emanating from the figure 8 solution. Several primary (BP or PD) bifurcation are necessary to connect the solution to the $m_1 = 0$ limit (RTBP). The family of relative equilibria emanating from the equilateral Lagrange solution (the lateral pointing triangles) is also displayed.

There is one further remarkable point which came out of our calculations. Chenciner and Montgomery [30] obtained the figure-8 orbit **A** by minimizing the action over a class of loops with some particular symmetry properties; the satellite
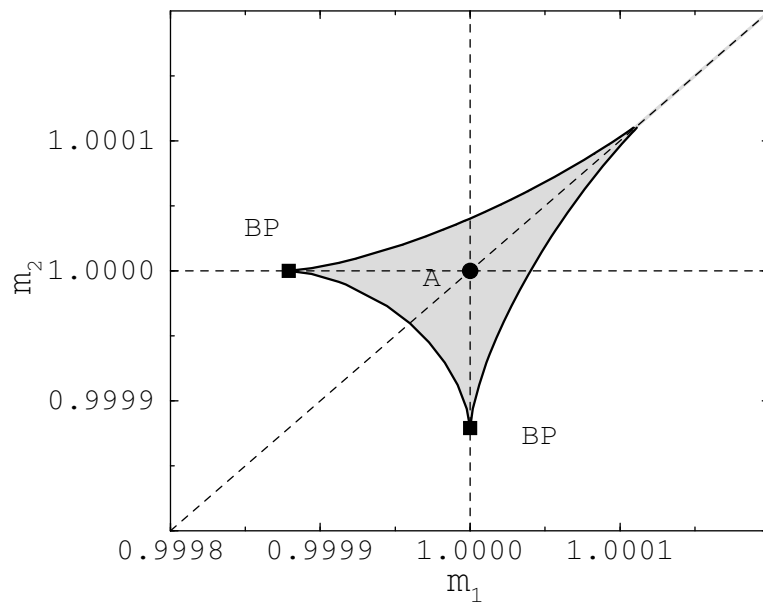
Fig. 11. Stability region in the (m_1, m_2)-plane for the continuation of the figure-8 solution.
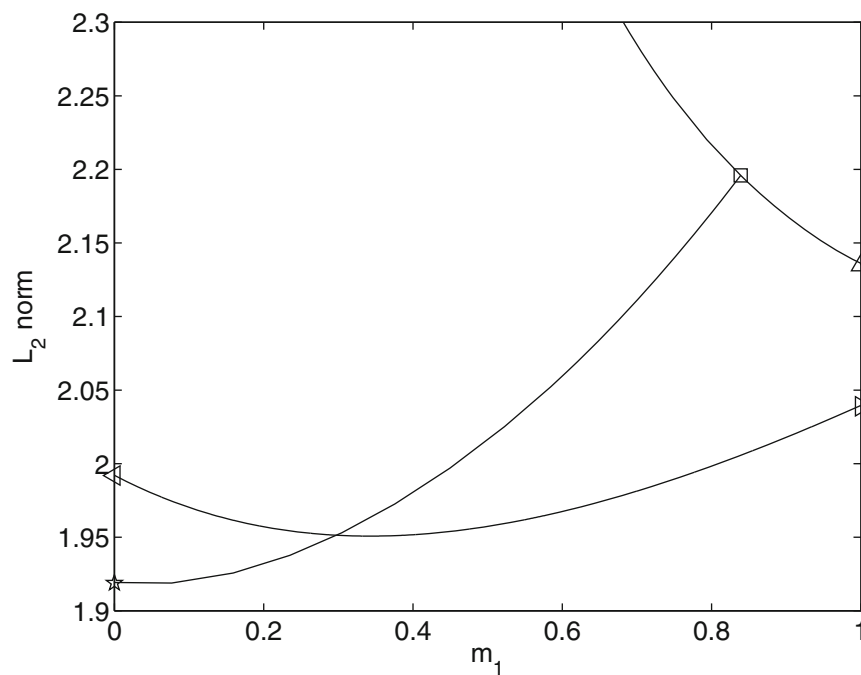

Fig. 12. Global bifurcation diagram of the family of periodic solutions emanating from the Fig. 8 solution. Several primary (BP or PD) bifurcation are necessary to connect the solution to the $m_1 = 0$ limit (RTBP). The family of relative equilibria emanating from the equilateral Lagrange solution (the lateral pointing triangles) is also displayed.

figure-8 solution **B** minimizes the action over a much larger class of paths. Therefore, the action corresponding to solution **B** should be less than or equal to the action corresponding to solution **A**. This is indeed the case, but in a rather unexpected way: within the precision of our calculations *both solutions have the same action*. Using the standard definition of the action and making the necessary normalisations the value of the action integral is for both solutions found to be equal to $S = 24.37197$. This surprising result reveals a degeneracy which deserves further analysis.

7 Conclusions

We have shown that continuation of solutions provides valuable information concerning the stability and bifurcation behavior of Hamiltonian systems. We have also established how two-point boundary value problem continuation software can be used to compute families of periodic solutions of symmetric Hamiltonian systems. The theory and the numerical implementations are well developed but not complete. Further work is necessary on the continuation of (1) relative equilibria in the non abelian case and (2) relative periodic orbits (see [37] for some progress in this direction). Also the use of reversibility properties in combination with the Hamiltonian structure needs further attention (see [38] and [15]).

References

1. H. Poincaré, *Les méthodes nouvelles de la mécanique céleste* (Gauthier-Villars, 1892)
2. M.C. Gutzwiller, *Chaos in Classical and Quantum Mechanics* (Springer Verlag, New York, 1990)
3. K.R. Meyer, J. Differ. Eqns. **39**, 2 (1981)
4. K.R. Meyer, G.R. Hall, *Introduction to Hamiltonian Dynamical Systems and the N-Body Problem.* Applied Mathematical Sciences 90 (Springer Verlag, New York, 1992)
5. B. Krauskop, H. Osinga, J. Galán-Vioque, *Numerical Continuation Methods for Dynamical Systems: Path following and boundary value problems* (Springer Verlag, Berlin, 2007)
6. C. Simó, In *Cent ans après les Méthodes Nouvelles de H. Poincaré* (Société Mathématique de France, 1996), p. 1
7. E.T. Whittaker, *A Treatise on the Analytical Dynamics of Particles & Rigid Bodies* (Cambridge University Press, 1947)
8. K.R. Meyer, *Periodic solutions of the N-body problem, Lecture Notes in Mathematics*, Vol. 1719 (Springer-Verlag, Berlin, 1999)
9. J. Sepulchre, R. MacKay, Nonlinearity **10**, 679 (1997)
10. A. Vanderbauwhede, Families of periodic orbits for autonomous systems. *Dynamical Systems II*, edited by A. Bednarek and L. Cesari (Academic Press, 1982), p. 427
11. J.A. Zufiría, *Symmetry Breaking of Water Waves*, Ph.D. Thesis, Applied Mathematics, Cal. Inst. of Technology, Pasadena, CA, 1987
12. D.G. Aronson, E.J. Doedel, H.G. Othmer, Int. J. Bifur. Chaos **1**, 1 (1991)
13. F.J. Muñoz-Almaraz, E. Freire, J. Galán, E.J. Doedel, A. Vanderbauwhede, Physica D **181**, 1 (2003)
14. J.S.W. Lamb, J.A.G. Roberts, Physica D **181**, 1 (2003)

15. F.J. Muñoz-Almaraz, E. Freire, J. Galán, A. Vanderbauwhede, Cel. Mech. Dyn. Astr. **97**, 17 (2007)
16. E.J. Doedel, Congr. Numer. **30**, 265 (1981)
17. E.J. Doedel, R. Paffenroth, A. Champneys, F. Fairgieve, Y.A. Kuznetsov, B. Oldeman, B. Sandstede, X. Wang, *AUTO2000: Continuation and bifurcation software for ordinary differential equations.* Department of Computer Science, Concordia University, Montreal, Canada, 2000, Website: `http://sourceforge.net/projects/auto2000/`
18. E.J. Doedel, H. Keller, J.P. Kernévez, Int. J. Bifur. Chaos **1**, 745 (1991)
19. R. Broucke, P.A. Baxa, Celestial Mech. **8**, 261 (1973)
20. J.P. van der Weele, E de Kleine, Physica A **228**, 245 (1996)
21. J.M. Tuwankotta, F. Verhulst, Siam J. Appl. Math. **61**, 1369 (2000)
22. F.J. Muñoz-Almaraz, J. Galán, E. Freire, Bifurcation behavior of the spring pendulum (preprint)
23. J.J. Morales-Ruiz, *Differential Galois Theory and Non-integrability of Hamiltonian Systems*, Progr. Math., 179 (Birkhäuser, 1999)
24. R. Barrio, F. Blesa, M. Lara, Comput. Math. Appl. **50**, 93 (2005) `http://gme.unizar.es/software/tides`
25. T. Doillet-Grellier, Master Thesis Engineering School University of Sevilla, 2012
26. A. Kremer, Master Thesis Engineering School University of Sevilla, 2012
27. A. Kremer, T. Doillet-Grellier, J. Galán, Evolution of a Poincaré Map for the Spring-Pendulum System, `www.youtube.com/watch?v=W_ym3RgD9Qg` (2012)
28. E.J. Doedel, R. Paffenroth, H. Keller, D. Dichmann, J. Galán-Vioque, A. Vanderbauwhede, Int. J. Bifur. Chaos **13**, 1353 (2003)
29. J. Galán, F.J. Muñoz-Almaraz, E. Freire, E.J. Doedel, A. Vanderbauwhede, Phys. Rev. Lett. **88**, 241101 (2002)
30. A. Chenciner, R. Montgomery, Ann. Math. **152**, 881 (2000)
31. C. Moore, Phys. Rev. Lett. **70**, 3675 (1993)
32. C. Simó, New families of solutions in n-body problems, In Proceedings ECM 2000, Barcelona (2000)
33. C. Simó, Contemp. Math. **292**, 209 (2002)
34. C. Marchal, Celestial Mech. Dyn. Astron. **78**, 279 (2000)
35. G.D. Birkhoff, Amer. Math. Soc. **29**, 1 (1927)
36. D. Offin, Instability for symmetric periodic solutions of the planar three body problem, Technical report, 2001
37. C. Wulff, A. Schebesch, J. Nonl. Science **18**, 343 (2008) `http://www.maths.surrey.ac.uk/personal/st/C.Wulff/publicationsframes.html`
38. F.J. Muñoz-Almaraz, *Continuación y bifurcaciones de órbitas periódicas en sistemas hamiltonianos con simetría*, Ph.D. thesis, Universidad de Sevilla, 2003